SCIENCE CHINA
Physics, Mechanics & Astronomy

• Article •
Editor's Focus

April 2021 Vol. 64 No. 4: 240362
https://doi.org/10.1007/s11433-021-1668-y

Editor's Focus

Electro-optic lithium niobate metasurfaces

BoFeng Gao[1], MengXin Ren[1,2*], Wei Wu[1], Wei Cai[1], and JingJun Xu[1*]

[1]*The Key Laboratory of Weak-Light Nonlinear Photonics, Ministry of Education, School of Physics and TEDA Applied Physics Institute, Nankai University, Tianjin 300071, China;*
[2]*Collaborative Innovation Center of Extreme Optics, Shanxi University, Taiyuan 030006, China*

Received January 20, 2021; accepted January 25, 2021; published online February 2, 2021

Many applications of metasurfaces require an ability to dynamically change their properties in the time domain. Electrical tuning techniques are of particular interest, since they pave a way to on-chip integration of metasurfaces with optoelectronic devices. In this work, we propose and experimentally demonstrate an electro-optic lithium niobate (EO-LN) metasurface that shows dynamic modulations to phase retardation of transmitted light. Quasi-bound states in the continuum (QBIC) are observed from this metasurface. By applying external electric voltages, the refractive index of lithium niobate (LN) is changed by Pockels EO nonlinearity, leading to efficient phase modulations to the transmitted light around the QBIC wavelength. The EO-LN metasurface developed in this study opens up new routes for potential applications in the field of displaying, pulse shaping, and spatial light modulating.

lithium niobate metasurfaces, electro-optic modulation, bound states in the continuum, resonance

PACS number(s): 42.70.Mp, 78.20.Jq, 42.70.-a, 42.25.-p

Citation: B. F. Gao, M. X. Ren, W. Wu, W. Cai, and J. J. Xu, Electro-optic lithium niobate metasurfaces, Sci. China-Phys. Mech. Astron. **64**, 240362 (2021), https://doi.org/10.1007/s11433-021-1668-y

1 Introduction

Formed by artificial subwavelength building blocks known as meta-atoms, metasurfaces have demonstrated their abilities to control optical waves with unprecedented flexibility and opened up our imagination for realizing a new generation of flat optical components outperforming their conventional bulky counterparts [1]. Despite their impressive advances, the current metasurfaces are mostly static in nature, with optical properties set in stone after the fabrication process. Realizing the modulation of metasurface properties in the time domain can provide new opportunities to manipulate light and thus facilitate a transition to dynamic optical devices [2-5]. For this purpose, different dynamic tuning mechanisms, such as optical pumping [6-10], thermal heating [11,12], chemical reaction [13,14], and electrical stimulation [15,16], have been implemented. Among all these tuning mechanisms, electrical tuning techniques are of particular interest, because they hold a promise to integrating metasurfaces with other on-chip optoelectronic devices. The most common electrical methods reported so far are based on triggering free carrier modulations [17-19], molecular reorientations [20], and phase transitions [21,22] in active materials integrated in the meta-atoms. However, the above approaches rely on relatively slow physical processes, and the switching time is commonly below nanosecond [23].

Lithium niobate (LN) is one of the most appealing materials to overcome this challenge. It shows an outstanding Pockels electro-optic (EO) effect, together with a refractive index changeable by an electrical voltage on the femtosec-

*Corresponding authors (MengXin Ren, email: ren_mengxin@nankai.edu.cn; JingJun Xu, email: jjxu@nankai.edu.cn)

ond timescale [24]. Thus LN enables optical modulators with much higher switching rates [25]. Recently, the thin-film LN on insulator (LNOI) [26,27] has emerged as a promising platform for ultracompact photonic devices [28-37]. Thanks to the large refractive index contrast between the LN film and substrate (such as silica), optical modes can be tightly confined within the nanometers-thin LN layer, leading to an improved EO modulation efficiency. And a variety of on-chip EO modulator units with tens to hundreds of GHz modulation speeds have been demonstrated using different LNOI microstructures, for example Mach-Zehnder interferometric waveguide [38, 39], photonic crystals [40, 41], micro-rings [42, 43] or micro-disks [44]. Recent years have witnessed significant advances in fabricating LN metasurfaces [45, 46] and consequently the demonstration of intriguing tunable second harmonic properties [47, 48]. However, the EO modulation by an LN metasurface, to the best of our knowledge, has rarely been experimentally explored.

A large EO modulation strength essentially implies sensitively tunable metasurface properties (such as phase retardation) by the EO-induced refractive index changes. For this purpose, an efficient way is to utilize high-quality factor (high-Q) resonant modes with a narrow spectra linewidth, which significantly elongate the effective optical path and photons lifetime in the meta-atoms, yielding enhanced local fields that experience the EO-refractive index changes. An attractive approach for the extremely high Q-factors is provided by the physics of bound states in the continuum (BICs). This concept was first proposed in quantum systems, where the electron wave function exhibits localization within the continuous spectrum of propagating waves [49, 50]. Recently, BICs have also attracted considerable attention in photonics [51-53]. Mathematically, the BICs show infinite Q-factors, where the optical energy is trapped without leakage [54, 55]. The ideal BICs have a vanishing spectral linewidth and are not observable in the electromagnetic spectra. However, in practice, introducing a structural asymmetry or oblique excitation could break the ideal BIC conditions [56, 57]. Consequently the perfect BIC modes will convert to quasi-BIC (QBIC) states that manifest themselves as extremely narrow spectral resonances with large Q-factors [58, 59]. Such QBICs have been observed in extended photonic systems and hold a great promise for various applications including vortex beam generation [60], nonlinear enhancement [61-63], low threshold lasing [64, 65], and sensitive sensing [66, 67].

In this paper, we numerically and experimentally demonstrate an LN metasurface offering EO phase modulation to transmitted light in the visible frequency regime. To yield an obvious phase modulation, we utilize a nanograting array under oblique incidence in which the EO effect induced by the applied bias voltage is significantly enhanced by leveraging the QBIC states, resulting in a 1.46 times larger EO modulation strength compared with the unstructured LN film. To the best of our knowledge, this is the first experimental demonstration of the EO modulation by the LN metasurfaces. Our results would act as a novel dynamic EO platform for wavefront engineering, pulse shaping, polarization control, etc.

2 Metasurface design and theoretical analysis

A design schematic of the EO-LN metasurface is shown in Figure 1. The metasurface is composed of an array of LN nanogratings residing on a fused quartz substrate. The LN ridge width is presented by d and grating period by D. Height h of 200 nm is determined by the thickness of the LN film (LNOI by NANOLN corporation) used for the metasurface fabrication. In our design, the orientation of the nanogratings is parallel to the e-axis of the LN crystal. And the external electric field is applied also along the e-axis to take advantage of the largest EO-coefficient element γ_{33}. We fabricate the metasurfaces by the focused ion beam technique (FIB, Ga^+, 30 kV, 40 pA) following the previous procedure [45]. Footprint of the metasurface array is 10 μm×10 μm. The Au electrodes with a 10 μm gap are fabricated via the standard UV-lithography procedure. Figure 1(b) gives the scanning electron microscope (SEM) images of total footprint and zoomed-in view of the fabricated LN-EO metasurface with D=390 nm and d=290 nm.

Figure 2(a) shows a full map of the transmission spectrum (T) of the metasurfaces with D=390 nm as a function of the incident angle (θ) under x-polarized incident light. The spectra are calculated using a finite element method (COMSOL Multiphysics). And ellipsometrically measured refractive indices of the birefringent LN and fused quartz are used in the simulations. Such grating structures are expected to support

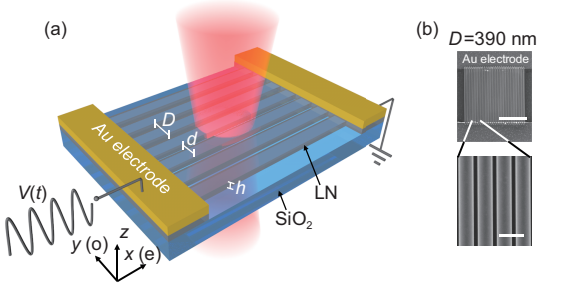

Figure 1 (Color online) Design of EO-LN metasurface. (a) Schematic illustration of the LN metasurface. The properties of the meta-atoms are actively modulated by applying an external electric voltage $V(t)$. The geometrical parameters of the metasurface include lattice constant D, ridge width d, and thickness h. (b) Scanning electron microscope images of the fabricated sample. Scale bars are 5 μm (up panel) and 500 nm (down panel), respectively.

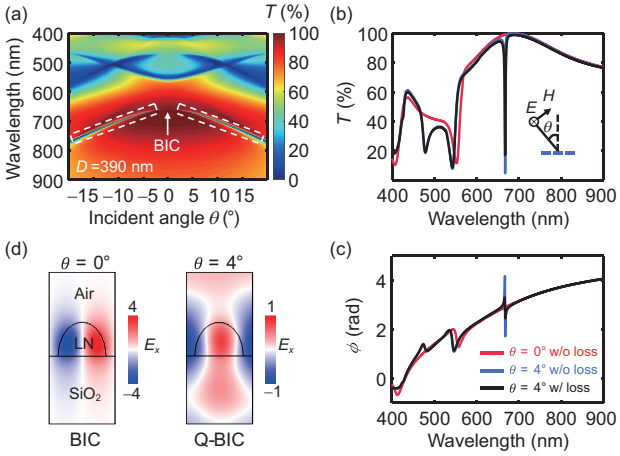

Figure 2 (Color online) BIC states in LN metasurface. (a) Incident-angle resolved transmission spectra of the LN metasurface. (b) Comparison of transmission T between 0° (red line) and 4° (blue and black lines) incidence shows a collapse of BIC to sharp Fano shaped QBIC resonance. The incident wave is polarized along the x-axis and located within the yoz-plane. The LN is assumed to be lossless for red and blue lines, while n_i is set as 0.002 to consider the loss caused by FIB fabrication (black line). (c) Spectra for transmitted phase ϕ. (d) Electric field distributions of eigenmodes for 0° and 4° incidence. The electric fields are tightly confined within the LN layer at 0°, while showing a clear leakage to air and SiO_2 substrate for 4° incidence.

the symmetry-protected BIC modes at normal incidence [52]. As shown in Figure 2(a), the resonant modes indicated by white dashed rectangles clearly emerge for oblique incidence (nonzero θ). In order to clarify the behavior of the BIC modes, we plot the transmission T and phase retardation (ϕ) spectra in Figure 2(b) and (c), respectively. It can be observed that ultra-narrow asymmetric Fano-shaped transmission dips and abrupt phase slips occur around the wavelength of 667 nm for incident angle of θ=4° (blue lines). These resonances vanish from the spectra at θ=0° (red curves). Such characteristic is clearly a manifestation of occurrence of the BIC resonant modes. Left panel of Figure 2(d) demonstrates the eigenmode distribution of the x-component of electric field (E_x) at θ=0° in the yoz cross section of the meta-atom. The mode exhibits an antisymmetric profile along the horizontal direction with a node formed at the center, corresponding to an odd mode parity symmetry. The electromagnetic fields are tightly confined in the LN layer and decoupled from the free-space propagating waves. However, for θ=4° the electric energy clearly leaks out into air and SiO_2 substrate, and the magnitude of the electric fields in the LN becomes 4 times weaker than the ideal BIC mode. Such phenomena further confirm the presence of the true BIC for normal incidence which collapses into the QBIC modes for oblique excitation. Although the LN is ideally lossless within the studied spectral range, the Ga^+ contamination and lattice damage during the FIB milling will inevitably deteriorate the optical performance of the metasurface [68]. Such influence is taken into account in the simulation by setting the imaginary part of the LN refractive index n_i as 0.002. The calculated results are shown by black curves. It can be clearly seen that the ultra-sharp dip in T and abrupt phase slip in ϕ are preserved, while the resonance strength in both T and ϕ is reduced owing to the optical loss.

Such high Q-factor QBIC resonance leads to an increased lifetime of photons and a strong localization of the fields within the meta-atoms, which would significantly enhance the light-matter interaction at the nanoscale and boost the spectral tunability resulting from the EO-induced refractive index change in the LN. It is worth noticing that the extremely sharp QBIC phase resonance can yield a substantial phase modulation in transmission through small EO spectral shifts of the modes. Figure 3 demonstrates the simulated phase spectra of the transmitted light through the metasurface for different variations in the real part of refractive index of the LN while maintaining n_i=0.002. It can be clearly observed that the phase spectrum shifts by 0.6 nm to shorter wavelengths for the reduced refractive index, while redshifts by the increased refractive index. The choice of operating wavelength at the QBIC resonance wavelength of 667 nm is denoted by the vertical dashed line in Figure 3(a). The phase modulation $\Delta\phi$ at this wavelength is calculated as a function of Δn and the results are plotted in Figure 3(b). It is shown that a modulation span $\Delta\phi$ of ±0.42 rad in the transmitted light phase is obtained through tuning QBIC resonance via a Δn modulation from –0.0025 to 0.0025.

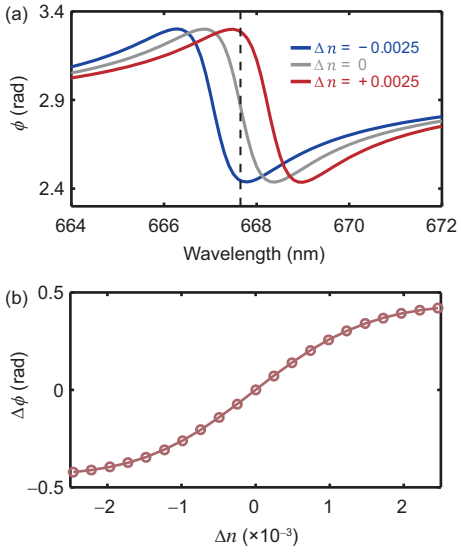

Figure 3 (Color online) Simulated EO-phase modulation by metasurface. (a) Transmission phase spectra of the LN metasurface with D=390 nm around QBIC wavelength (indicated by vertical dashed line) for 4° oblique incidence corresponding to different refractive index modulations. (b) Relation between transmitted phase modulation and refractive index modulation for the LN metasurface at the QBIC wavelength.

3 Experimental characterization

To experimentally evaluate the transmission spectrum of the fabricated LN metasurface, we build a micro-spectrometer. The output of a supercontinuum laser (NKT EXR-15) is focused onto the LN metasurfaces by a 10× objective forming a convergent beam with a convergence angle of about 13°. The transmitted light is analyzed using a spectrometer (Horiba MicroHR). The measured transmission spectrum under x-polarized incidence is given in Figure 4(b). A QBIC resonance dip clearly appears around 633 nm, as indicated by a vertical black arrow. It is shown that the experimentally measured QBIC resonance is much shallower and broader leading to a smaller Q-factor compared with the simulation results shown in Figure 2. Such discrepancy could be explained by the fabrication imperfections. Furthermore, both normal and oblique incidence components are included in the experiment, thus the QBIC dip may be averaged out by the normal incident component.

The EO phase modulation by the metasurfaces is characterized by a home-built laser heterodyne detection system (shown in Figure 4(a)). An x-polarized 633 nm continuous wave laser (CNILaser, MGL-III-532) is launched into an acoustic-optic frequency shifter (AOFS) and divided into two parts, i.e., the 0th order transmitted and the 1st order diffracted light beams. The 0th order light without frequency shift is used as probe light to focus onto the LN metasurface by the 10× objective. The 1st order light with a frequency downshift of f_c=110 MHz is used as reference light. An arbitrary waveform generator (Agilent 33250A) is used to generate a sinusoidal driving voltage signal at f_m=1.0 MHz, which is further amplified to be 300 V_{pp} (peak-to-peak magnitude, –150 V to +150 V output voltage) using a high-voltage amplifier (Falco Corp.), and then fed into the electrodes. As a consequence, the phase of the probe light is changed by the EO response of the LN metasurface. After interfering the probe light with the reference beam, optical beats are generated and subsequently recorded by a photodetector and an RF spectrum analyzer. In the measurements, the visibility of the optical beats is optimized by equilibrating the powers and optical paths of the two beams.

Assuming the probe and reference beams at the photodetector are $E_p = e^{i[2\pi f_o t + m\sin(2\pi f_m t)]}$ and $E_r = e^{i2\pi(f_o - f_c)t}$, respectively where f_o is the optical frequency of the 633 nm laser, and m is the EO phase modulation magnitude. Thus the optical beats can be described as $I = |E_p + E_r|^2 =$

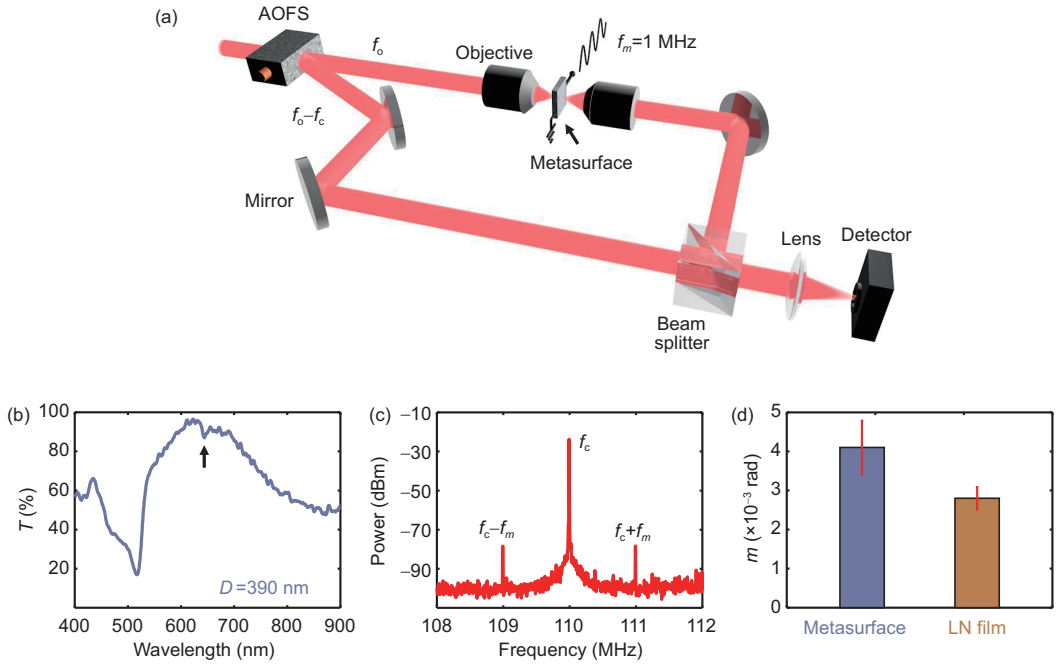

Figure 4 (Color online) Experimental EO phase modulation by metasurface. (a) A schematic diagram of a laser heterodyne detection system. An acoustic-optic frequency shifter (AOFS) is used to divide an input 633 nm laser (with optical frequency of f_o) into two parts. The 0th order light is used as probe light to excite the LN metasurface. The frequency of the 1st order light is downshifted by f_c=110 MHz and used as reference light. The metasurface is modulated by a sinusoidal electric voltage at f_m=1.0 MHz. (b) Experimentally measured transmission spectrum of the metasurface with D=390 nm excited by focused light with a convergence angle of about 13°. A clear QBIC resonance dip is observed around 633 nm as indicated by a vertical black arrow. (c) Power spectrum of optical beats recorded by an RF spectrum analyzer. Three distinct peaks are observed at $f_c - f_m$=109 MHz, f_c=110 MHz and $f_c + f_m$=111 MHz. (d) Phase modulation magnitude m measured from the LN metasurface and the unstructured LN film. Heights of histograms are the average values of multiple measurements, and error bars are their standard deviations.

$2+2\cos[2\pi f_c t+m\sin(2\pi f_m t)]$. When $m \ll 1$, such beat signal could be expressed by a set of standard Bessel function expansions $I = 2+2\{J_0(m)\cos(2\pi f_c t)+J_1(m)[\cos(2\pi(f_c+f_m)t)-\cos(2\pi(f_c-f_m)t)]\}$, and the corresponding Fourier frequency spectrum can be expressed as $\mathcal{F}(f) = 2\delta(f) + J_0(m)\delta(f - f_c) + J_1(m)[\delta(f-(f_c+f_m)) - \delta(f-(f_c-f_m))]$, in which $\delta(f)$ is the Kronecker delta function [69]. This equation indicates that the phase modulation signal results in three discrete frequency components $f_c - f_m$, f_c and $f_c + f_m$, respectively. As shown in Figure 4(c), three distinct peaks are observed at 109, 110 and 111 MHz in the experimental power spectrum. The magnitude of the frequency component at f_c and $f_c \pm f_m$ is proportional to $J_0^2(m)$ and $J_1^2(m)$, respectively. Then the phase modulation magnitude m can be mathematically demodulated by the experimental ratio of $J_0^2(m)/J_1^2(m)$. The deduced m for the metasurface and the unstructured LN film are shown in Figure 4(d), in which the heights of histograms are the average m values of multiple measurements, and error bars are their standard deviations. The m of 0.0041 rad is achieved from the metasurface, which is larger than 0.0028 rad by the unstructured LN film. This explicitly shows that the metasurface is a good candidate for stronger EO-modulation.

4 Conclusions

In conclusion, we have numerically and experimentally demonstrated an EO tunable LN metasurface that provides a dynamic control over the phase retardation of transmitted light in the visible spectral regime. The oblique incidence enables collapse of symmetry-protected BICs into Fano resonant QBIC modes with ultrahigh Q-factors, which significantly increases the lifetime of photons as well as field confinement within the resonators, ultimately leading to an improved modulation sensitivity. The proposed EO-LN metasurface is a good candidate for developing multifunctional and tunable optical components such as ultracompact spatial light modulators and optical switches, and will find various applications in displaying, optical wavefront shaping, and so on.

This work was supported by the Guangdong Major Project of Basic and Applied Basic Research (Grant No. 2020B0301030009), the National Key R&D Program of China (Grant Nos. 2017YFA0305100, 2017YFA0303800, and 2019YFA0705000), the National Natural Science Foundation of China (Grant Nos. 92050114, 91750204, 61775106, 11904182, 12074200, and 11774185), the 111 Project (Grant No. B07013), PCSIRT (Grant No. IRT0149), the Open Research Program of Key Laboratory of 3D Micro/Nano Fabrication and Characterization of Zhejiang Province, Fundamental Research Funds for the Central Universities (Grant Nos. 010-63201003, 010-63201008, and 010-63201009), and Tianjin Youth Talent Support Program. We thank the Nanofabrication Platform of Nankai University for fabricating the samples.

1 N. I. Zheludev, and Y. S. Kivshar, Nat. Mater. **11**, 917 (2012).
2 G. Li, S. Zhang, and T. Zentgraf, Nat. Rev. Mater. **2**, 17010 (2017).
3 A. M. Shaltout, V. M. Shalaev, and M. L. Brongersma, Science **364**, eaat3100 (2019).
4 Q. He, S. Sun, and L. Zhou, Research **2019**, 1 (2019).
5 M. Ren, W. Cai, and J. Xu, Adv. Mater. **32**, 1806317 (2020).
6 Q. Wang, G. H. Yuan, K. S. Kiang, K. Sun, B. Gholipour, E. T. F. Rogers, K. Huang, S. S. Ang, N. I. Zheludev, and J. H. Teng, Appl. Phys. Lett. **110**, 201110 (2017).
7 M. Taghinejad, H. Taghinejad, Z. Xu, K. T. Lee, S. P. Rodrigues, J. Yan, A. Adibi, T. Lian, and W. Cai, Nano Lett. **18**, 5544 (2018).
8 M. X. Ren, W. Wu, W. Cai, B. Pi, X. Z. Zhang, and J. J. Xu, Light Sci. Appl. **6**, e16254 (2017).
9 L. H. Nicholls, F. J. Rodríguez-Fortuño, M. E. Nasir, R. M. Córdova-Castro, N. Olivier, G. A. Wurtz, and A. V. Zayats, Nat. Photon. **11**, 628 (2017).
10 C. Guan, J. Shi, J. Liu, H. Liu, P. Li, W. Ye, and S. Zhang, Laser Photon. Rev. **13**, 1800242 (2019).
11 J. Y. Ou, E. Plum, L. Jiang, and N. I. Zheludev, Nano Lett. **11**, 2142 (2011).
12 X. Yin, M. Schäferling, A. K. U. Michel, A. Tittl, M. Wuttig, T. Taubner, and H. Giessen, Nano Lett. **15**, 4255 (2015).
13 G. Di Martino, S. Tappertzhofen, S. Hofmann, and J. Baumberg, Small **12**, 1334 (2016).
14 X. Duan, S. Kamin, and N. Liu, Nat. Commun. **8**, 14606 (2017).
15 Z. L. Sámson, K. F. MacDonald, F. De Angelis, B. Gholipour, K. Knight, C. C. Huang, E. Di Fabrizio, D. W. Hewak, and N. I. Zheludev, Appl. Phys. Lett. **96**, 143105 (2010), arXiv: 0912.4288.
16 A. Karvounis, V. V. Vogler-Neuling, F. U. Richter, E. Dénervaud, M. Timofeeva, and R. Grange, Adv. Opt. Mater. **8**, 2000623 (2020).
17 M. M. Salary, A. Forouzmand, and H. Mosallaei, ACS Photon. **4**, 63 (2017).
18 H. T. Chen, W. J. Padilla, J. M. O. Zide, A. C. Gossard, A. J. Taylor, and R. D. Averitt, Nature **444**, 597 (2006).
19 N. Dabidian, I. Kholmanov, A. B. Khanikaev, K. Tatar, S. Trendafilov, S. H. Mousavi, C. Magnuson, R. S. Ruoff, and G. Shvets, ACS Photon. **2**, 216 (2015).
20 M. Decker, C. Kremers, A. Minovich, I. Staude, A. E. Miroshnichenko, D. Chigrin, D. N. Neshev, C. Jagadish, and Y. S. Kivshar, Opt. Express **21**, 8879 (2013), arXiv: 1302.4484.
21 T. Driscoll, H. T. Kim, B. G. Chae, B. J. Kim, Y. W. Lee, N. M. Jokerst, S. Palit, D. R. Smith, M. Di Ventra, and D. N. Basov, Science **325**, 1518 (2009), arXiv: 1003.0140.
22 Z. Y. Jia, F. Z. Shu, Y. J. Gao, F. Cheng, R. W. Peng, R. H. Fan, Y. Liu, and M. Wang, Phys. Rev. Appl. **9**, 034009 (2018).
23 J. Lee, S. Jung, P. Y. Chen, F. Lu, F. Demmerle, G. Boehm, M. C. Amann, A. Alú, and M. A. Belkin, Adv. Opt. Mater. **2**, 1057 (2014).
24 G. Gaborit, J. Dahdah, F. Lecoche, P. Jarrige, Y. Gaeremynck, E. Duraz, and L. Duvillaret, IEEE Trans. Plasma Sci. **41**, 2851 (2013).
25 T. S. El-Bawab, *Optical Switching* (Springer Science & Business Media, Heidelberg, 2008).
26 M. Levy, R. M. Osgood Jr., R. Liu, L. E. Cross, G. S. Cargill Iii, A. Kumar, and H. Bakhru, Appl. Phys. Lett. **73**, 2293 (1998).
27 P. Rabiei, and P. Gunter, Appl. Phys. Lett. **85**, 4603 (2004).
28 G. Poberaj, H. Hu, W. Sohler, and P. Günter, Laser Photon. Rev. **6**, 488 (2012).
29 Z. Fang, Y. Xu, M. Wang, L. Qiao, J. Lin, W. Fang, and Y. Cheng, Sci. Rep. **7**, 45610 (2017), arXiv: 1701.05374.
30 Y. Kong, F. Bo, W. Wang, D. Zheng, H. Liu, G. Zhang, R. Rupp, and J. Xu, Adv. Mater. **32**, 1806452 (2020).
31 D. Sun, Y. Zhang, D. Wang, W. Song, X. Liu, J. Pang, D. Geng, Y. Sang, and H. Liu, Light Sci. Appl. **9**, 197 (2020).

32 M. Yu, Y. Okawachi, R. Cheng, C. Wang, M. Zhang, A. L. Gaeta, and M. Lončar, Light Sci. Appl. **9**, 9 (2020), arXiv: 1909.00249.
33 Y. A. Liu, X. S. Yan, J. W. Wu, B. Zhu, Y. P. Chen, and X. F. Chen, Sci. China-Phys. Mech. Astron. **64**, 234262 (2021), arXiv: 2009.12900.
34 Q. Luo, Z. Z. Hao, C. Yang, R. Zhang, D. H. Zheng, S. G. Liu, H. D. Liu, F. Bo, Y. F. Kong, G. Q. Zhang, and J. J. Xu, Sci. China-Phys. Mech. Astron. **64**, 234263 (2021).
35 G. L. Long, Sci. China-Phys. Mech. Astron. **64**, 234261 (2021).
36 J. T. Lin, Y. X. Xu, Z. W. Fang, M. Wang, N. W. Wang, L. L. Qiao, W. Fang, and Y. Cheng, Sci. China-Phys. Mech. Astron. **58**, 114209 (2015), arXiv: 1405.6473.
37 M. Wang, R. Wu, J. Lin, J. Zhang, Z. Fang, Z. Chai, and Y. Cheng, Quantum Eng. **1**, e9 (2019).
38 C. Wang, M. Zhang, X. Chen, M. Bertrand, A. Shams-Ansari, S. Chandrasekhar, P. Winzer, and M. Lončar, Nature **562**, 101 (2018).
39 M. He, M. Xu, Y. Ren, J. Jian, Z. Ruan, Y. Xu, S. Gao, S. Sun, X. Wen, L. Zhou, L. Liu, C. Guo, H. Chen, S. Yu, L. Liu, and X. Cai, Nat. Photon. **13**, 359 (2019), arXiv: 1807.10362.
40 T. Ding, Y. Zheng, and X. Chen, Opt. Lett. **44**, 1524 (2019).
41 M. Li, J. Ling, Y. He, U. A. Javid, S. Xue, and Q. Lin, Nat. Commun. **11**, 1 (2020).
42 A. Guarino, G. Poberaj, D. Rezzonico, R. Degl'Innocenti, and P. Günter, Nat. Photon. **1**, 407 (2007), arXiv: 0705.2392.
43 M. Zhang, B. Buscaino, C. Wang, A. Shams-Ansari, C. Reimer, R. Zhu, J. M. Kahn, and M. Lončar, Nature **568**, 373 (2019), arXiv: 1809.08636.
44 F. Bo, J. Wang, J. Cui, S. K. Ozdemir, Y. Kong, G. Zhang, J. Xu, and L. Yang, Adv. Mater. **27**, 8075 (2015).
45 B. Gao, M. Ren, W. Wu, H. Hu, W. Cai, and J. Xu, Laser Photon. Rev. **13**, 1800312 (2019), arXiv: 1810.11928.
46 B. Fang, H. Li, S. Zhu, and T. Li, Photon. Res. **8**, 1296 (2020).
47 J. Ma, M. Ren, W. Wu, W. Cai, and J. Xu, arXiv: 2002.06594.
48 A. Fedotova, M. Younesi, J. Sautter, A. Vaskin, F. J. F. Löchner, M. Steinert, R. Geiss, T. Pertsch, I. Staude, and F. Setzpfandt, Nano Lett. **20**, 8608 (2020).
49 J. Von Neuman, and E. Wigner, Phys. Z **30**, 465 (1929).
50 H. Friedrich, and D. Wintgen, Phys. Rev. A **32**, 3231 (1985).
51 D. C. Marinica, A. G. Borisov, and S. V. Shabanov, Phys. Rev. Lett. **100**, 183902 (2008).
52 C. W. Hsu, B. Zhen, A. D. Stone, J. D. Joannopoulos, and M. Soljačić, Nat. Rev. Mater. **1**, 16048 (2016).
53 M. Wang, Y. Z. Wang, X. S. Xu, Y. Q. Hu, and G. L. Long, Opt. Express **27**, 63 (2019).
54 K. Koshelev, S. Lepeshov, M. Liu, A. Bogdanov, and Y. Kivshar, Phys. Rev. Lett. **121**, 193903 (2018), arXiv: 1809.00330.
55 J. Xiang, Y. Xu, J. D. Chen, and S. Lan, Nanophotonics **9**, 133 (2020).
56 Z. Liu, Y. Xu, Y. Lin, J. Xiang, T. Feng, Q. Cao, J. Li, S. Lan, and J. Liu, Phys. Rev. Lett. **123**, 253901 (2019).
57 Z. Huang, M. Wang, Y. Li, J. Shang, K. Li, W. Qiu, J. Dong, H. Guan, Z. Chen, and H. Lu, arXiv: 2006.10908.
58 S. I. Azzam, V. M. Shalaev, A. Boltasseva, and A. V. Kildishev, Phys. Rev. Lett. **121**, 253901 (2018), arXiv: 1808.08244.
59 S. Han, L. Cong, Y. K. Srivastava, B. Qiang, M. V. Rybin, A. Kumar, R. Jain, W. X. Lim, V. G. Achanta, S. S. Prabhu, Q. J. Wang, Y. S. Kivshar, and R. Singh, Adv. Mater. **31**, 1901921 (2019).
60 B. Wang, W. Liu, M. Zhao, J. Wang, Y. Zhang, A. Chen, F. Guan, X. Liu, L. Shi, and J. Zi, Nat. Photon. **14**, 623 (2020), arXiv: 1909.12618.
61 L. Carletti, K. Koshelev, C. De Angelis, and Y. Kivshar, Phys. Rev. Lett. **121**, 033903 (2018), arXiv: 1804.02947.
62 S. D. Krasikov, A. A. Bogdanov, and I. V. Iorsh, Phys. Rev. B **97**, 224309 (2018), arXiv: 1803.10980.
63 A. P. Anthur, H. Zhang, R. Paniagua-Dominguez, D. A. Kalashnikov, S. T. Ha, T. W. W. Maβ, A. I. Kuznetsov, and L. Krivitsky, Nano Lett. **20**, 8745 (2020).
64 A. Kodigala, T. Lepetit, Q. Gu, B. Bahari, Y. Fainman, and B. Kanté, Nature **541**, 196 (2017), arXiv: 1508.05164.
65 C. Huang, C. Zhang, S. Xiao, Y. Wang, Y. Fan, Y. Liu, N. Zhang, G. Qu, H. Ji, J. Han, L. Ge, Y. Kivshar, and Q. Song, Science **367**, 1018 (2020).
66 S. Romano, G. Zito, S. Torino, G. Calafiore, E. Penzo, G. Coppola, S. Cabrini, I. Rendina, and V. Mocella, Photon. Res. **6**, 726 (2018).
67 A. Leitis, A. Tittl, M. Liu, B. H. Lee, M. B. Gu, Y. S. Kivshar, and H. Altug, Sci. Adv. **5**, eaaw2871 (2019).
68 R. Geiss, S. Diziain, M. Steinert, F. Schrempel, E. B. Kley, A. Tünnermann, and T. Pertsch, Phys. Status Solidi A **211**, 2421 (2014).
69 W. Zhang, W. Gao, L. Huang, D. Mao, B. Jiang, F. Gao, D. Yang, G. Zhang, J. Xu, and J. Zhao, Opt. Express **23**, 17576 (2015).